

LETTER • OPEN ACCESS

## 4DEnVar-based inversion system for ammonia emission estimation in China through assimilating IASI ammonia retrievals

To cite this article: Jianbing Jin *et al* 2023 *Environ. Res. Lett.* **18** 034005

View the [article online](#) for updates and enhancements.

You may also like

- [Global, regional and national trends of atmospheric ammonia derived from a decadal \(2008–2018\) satellite record](#)  
Martin Van Damme, Lieven Clarisse, Bruno Franco et al.
- [Ammonia Electrolysis in a Municipal Wastewater Treatment Plant](#)  
Gerardine G Botte
- [What is the real utility of breath ammonia concentration measurements in medicine and physiology?](#)  
Patrik Španl and David Smith

ENVIRONMENTAL RESEARCH  
LETTERS

## LETTER

## OPEN ACCESS

RECEIVED  
23 August 2022REVISED  
29 January 2023ACCEPTED FOR PUBLICATION  
2 February 2023PUBLISHED  
14 February 2023

Original Content from  
this work may be used  
under the terms of the  
[Creative Commons  
Attribution 4.0 licence](#).

Any further distribution  
of this work must  
maintain attribution to  
the author(s) and the title  
of the work, journal  
citation and DOI.

4DEnVar-based inversion system for ammonia emission  
estimation in China through assimilating IASI ammonia retrievalsJianbing Jin<sup>1</sup> , Li Fang<sup>1</sup>, Baojie Li<sup>1</sup>, Hong Liao<sup>1,\*</sup>, Ye Wang<sup>1</sup>, Wei Han<sup>2</sup>, Ke Li<sup>1</sup> , Mijie Pang<sup>1</sup> , Xingyi Wu<sup>1</sup>  
and Hai Xiang Lin<sup>3,4</sup> <sup>1</sup> Jiangsu Key Laboratory of Atmospheric Environment Monitoring and Pollution Control, Collaborative Innovation Center of Atmospheric Environment and Equipment Technology, School of Environmental Science and Engineering, Nanjing University of Information Science and Technology, Nanjing, People's Republic of China<sup>2</sup> Numerical Weather Prediction Center, Chinese Meteorological Administration, Beijing, People's Republic of China<sup>3</sup> Institute of Environmental Sciences, Leiden University, Leiden, The Netherlands<sup>4</sup> Delft Institute of Applied Mathematics, Delft University of Technology, Delft, The Netherlands

\* Author to whom any correspondence should be addressed.

E-mail: [hongliao@nuist.edu.cn](mailto:hongliao@nuist.edu.cn)

Keywords: atmospheric ammonia, emission inversion, IASI

Supplementary material for this article is available [online](#)

## Abstract

Atmospheric ammonia has been hazardous to the environment and human health for decades. Current inventories are usually constructed in a bottom-up manner and subject to uncertainties and incapable of reproducing the spatiotemporal characteristics of ammonia emission. Satellite measurements, for example, Infrared Atmospheric Sounder Interferometer (IASI) and Cross-Track Infrared Sounder, which provide global coverage of ammonia distribution, have gained popularity in ammonia emission estimation through data assimilation methods. However, satellite-based emission inversion studies on China are limited. In this study, we propose a four-dimensional ensemble variational-based ammonia emission inversion system to optimize ammonia emissions in China. It was developed by assimilating the IASI ammonia retrievals onboard Meteorological Operational satellite A and B into a chemical transport model Goddard Earth Observing System Chemical model (GEOS-Chem). Monthly inversion experiments were conducted in April, July, and October 2016 to test the performance. The inversion result indicated that the prior inventory from the MEIC model captured ammonia spreads in general; however, it heterogeneously underrated the emission intensity. The increments obtained in the assimilation were as high as 50% in North, East, and Northwest China. The posterior emission inventory presented a regional emission flux consistent with relevant studies. Driven by the optimized source estimate, GEOS-Chem provides superior results than using the prior in the evaluation of the assimilated IASI retrievals and the surface ammonia concentration measured by the ground-based Ammonia Monitoring Network in China.

## 1. Introduction

As an abundant nitrogen species, atmospheric ammonia (NH<sub>3</sub>) is highly reactive and readily reacts with acids, such as H<sub>2</sub>SO<sub>4</sub> and HNO<sub>3</sub>. The formation of secondary fine particulate matter (PM<sub>2.5</sub>) poses significant threat to public health (Huang *et al* 2014) and plays a vital role in global climate change (Myhre *et al* 2013). In addition, excess deposition of reactive

nitrogen is associated with soil acidification, eutrophication (Krupa 2003), and ecosystem imbalance (Hernández *et al* 2016). Atmospheric NH<sub>3</sub> is primarily attributed to agricultural, industrial, and traffic sources (Li *et al* 2021). As a country with an enormous livestock population and tremendous nitrogen fertilizer and fossil fuel consumption, China has been affected by the high-level atmospheric NH<sub>3</sub> over the past two decades (Huang *et al* 2012, Pan *et al* 2018).

Over the last decade, significant efforts have been made to quantify the spatiotemporal distribution of ammonia sources and develop global emission inventories, such as the Emissions Database for Global Atmospheric Research (Crippa *et al* 2018), the Community Emissions Data System (CEDS) (Hoesly *et al* 2018), and regional NH<sub>3</sub> inventories over China (Huang *et al* 2012, Kang *et al* 2016, Xu *et al* 2016, Zhou *et al* 2016, Zhang *et al* 2018). Driven by these ammonia source datasets, various numerical chemical transport models, such as Goddard Earth Observing System Chemical model (GEOS-Chem) (Walker *et al* 2012) and WRF-Chem (Li *et al* 2021), have been used to reproduce the ammonia life cycles of chemical reactions, transport, and wet/dry sinks. These models not only help to better quantify the environmental impact of atmospheric ammonia but are also essential tools for evaluating future ammonia emission reduction strategies. However, large uncertainties are present in these bottom-up ammonia emission sources (Xu *et al* 2019). As reported by Zhang *et al* (2018), the difference between the current estimates of agricultural ammonia emissions in China can be as high as a factor of 2. Take year of 2008 for instance, the total anthropogenic NH<sub>3</sub> emissions over China ranged from 8.4 to 15.0 Tg in different estimates (Kurokawa *et al* 2013, Paulot *et al* 2014, Xu *et al* 2016). The large discrepancies mislead the modeling results and, consequently, our understanding of their environmental impact.

Continuous advances in sensor techniques have made the large-scale observation of ammonia feasible. Limited ground-based observations are available for measuring ammonia levels in China. An ammonia monitoring network covering 53 sites was developed by Pan *et al* (2018). However, the observational campaign only lasted for 1 year. In contrast, satellite-based remote sensing instruments, such as the tropospheric emission spectrometer (TES) (Beer *et al* 2008), cross-track infrared sounder (CrIS) (Shepherd and Cady-Pereira 2015), and infrared atmospheric sounder interferometers (IASI) (Clarisse *et al* 2009), have gained popularity and have been used alongside numerical models to analyze ammonia (Ge *et al* 2020). Despite their significant roles in characterizing ammonia, these measurements are not sufficient to provide complete insight into ammonia. This is because these observations do not reflect the emission intensity directly, only report vertically integrated quantities (satellite-based data) or cover a very limited area (surface observing network).

Instead of exploring atmospheric ammonia cycles with simulation models or observations alone, data assimilation was used to combine them to fill in observation and simulation gaps (Kalnay 2002). Data assimilation could nudge parameters or states with an allowed range, such that the simulation better

fit the measurements. For ammonia application, assimilation is usually performed to calculate the most likely emission field, and this top-down method is referred to as *ammonia emission inversion*. Atmospheric ammonia emission inversion has recently attracted considerable attention worldwide. For instance, Cao *et al* (2020, 2022) conducted a 4DVar-based inversion using CrIS retrieval data and the GEOS-Chem model to optimize the monthly ammonia emission inventories in Europe and the US. CrIS measurements were also assimilated to constrain the ammonia source inventory over North America in Sitwell *et al* (2022) and Europe in van der Graaf *et al* (2022). The IASI ammonia column concentrations were used by Chen *et al* (2021) for the US ammonia emission estimation.

However, studies on ammonia emission inversion focusing on China are limited. To the best of our knowledge, only three studies (Paulot *et al* 2014, Zhang *et al* 2018, Kong *et al* 2019) have been conducted to date. In Paulot *et al* (2014), indirect measurements and nitrogen deposition from very few monitoring stations (30 sites) were assimilated to update ammonia emissions in Asia from 2005 to 2008. Recently, Kong *et al* (2019) used ground-based ammonia concentrations from the Ammonia Monitoring Network in China (Amon-China, 53 sites) (Pan *et al* 2018) and updated the Chinese ammonia emission inventory in 2016. Nevertheless, both observational networks had limited sites; hence, they could not fully capture the high spatial variability of ammonia throughout China. Additionally, their observational campaign was conducted over a short period and was no longer in operation, and therefore helped little in the temporal profile of annual ammonia variation. The first satellite observations of tropospheric ammonia (TES) were assimilated by Zhang *et al* (2018). Their emission inversion was only conducted to estimate ammonia emissions in China in 2008. Launched in 2004 and ending its mission in 2018, the TES mission had much less spatial coverage than the IASI, especially in its later years (Guo *et al* 2021). New IASI and CrIS instruments, which have better spatial coverage and higher resolution, are recommended for characterizing global or regional ammonia source distributions (Zhang *et al* 2018).

Compared to the nitrogen deposition and concentration measurements from limited ground-based observation sites and the coarse-resolution TES satellite ammonia retrievals, the identical IASI instruments onboard Metop-A (operated from 2008 to 2018), Metop-B (from 2012), and Metop-C (from 2018) satellites provide better spatiotemporal coverage and higher resolution of ammonia in the past decade. In this study, we introduced an inversion system for long-term ammonia emission estimation in China. It was developed by feeding IASI ammonia

measurements into the GEOS-Chem model using a four-dimensional ensemble variational (4D-EnVar) data assimilation algorithm. The emission inversion system was first tested in 2016 for this study, as its effectiveness could be evaluated with emission results reported in relevant studies (Kong *et al* 2019, Li *et al* 2021) and the independent ammonia concentration measurements collected in Pan *et al* (2018), whereas the long-term annual/seasonal variation of ammonia emissions will be explored in our next work. CrIS instrument also provides high-quality ammonia observations over the past decades, and the assimilation of its product will be considered in our future study as well. The proposed inversion system will not only promote the development of ammonia emission inventories, but also improve our understanding of atmospheric ammonia life cycles in China and help obtain a better assessment of their environmental influences.

The remainder of this paper is organized as follows. Section 2 introduces the GEOS-Chem chemical transport model for ammonia simulations. The IASI ammonia total column measurements for assimilation and ammonia surface concentration for independent evaluation are also illustrated. The ammonia emission inversion system was designed, and the assimilation and local analysis algorithms are discussed in section 3. The posterior emission field, the simulated total ammonia column and surface concentration are evaluated and discussed in section 4. Section 5 summarizes the conclusion and the added value of the top-down inversion method to resolve the uncertainty in the emission inventory and introduces our future work.

## 2. Ammonia simulation and observation

### 2.1. GEOS-Chem model

To simulate atmospheric ammonia in the modelling domain shown in figure 1, we ran a nested grid simulation in GEOS-Chem model v13.3.3. Global simulations with a horizontal resolution of  $2^\circ$  latitude by  $2.5^\circ$  longitude as the boundary condition were taken every 3 h. The nested domain ( $72^\circ$ – $136^\circ$  E,  $17.5^\circ$ – $54^\circ$  N) has a horizontal resolution of  $0.5^\circ$  latitude by  $0.625^\circ$  longitude and 47 vertical layers. The reanalysis meteorological field to drive GEOS-Chem in this work was from the Modern-Era Retrospective Analysis for Research and Applications, version 2 (MERRA-2) meteorological field (Gelaro *et al* 2017). Each simulation had a spin-up period of 6 months.

GEOS-Chem has a fully coupled aerosol-ozone- $\text{NO}_x$ -hydrocarbon chemistry representation (Park *et al* 2004). The wet deposition scheme for soluble aerosols and gases was described in Liu *et al* (2001) and the dry deposition scheme was described in Zhang *et al* (2001). In the model configuration, the

time steps for dynamics and chemistry were 600 and 1200 s, respectively.

### 2.2. Prior anthropogenic $\text{NH}_3$ emission inventory

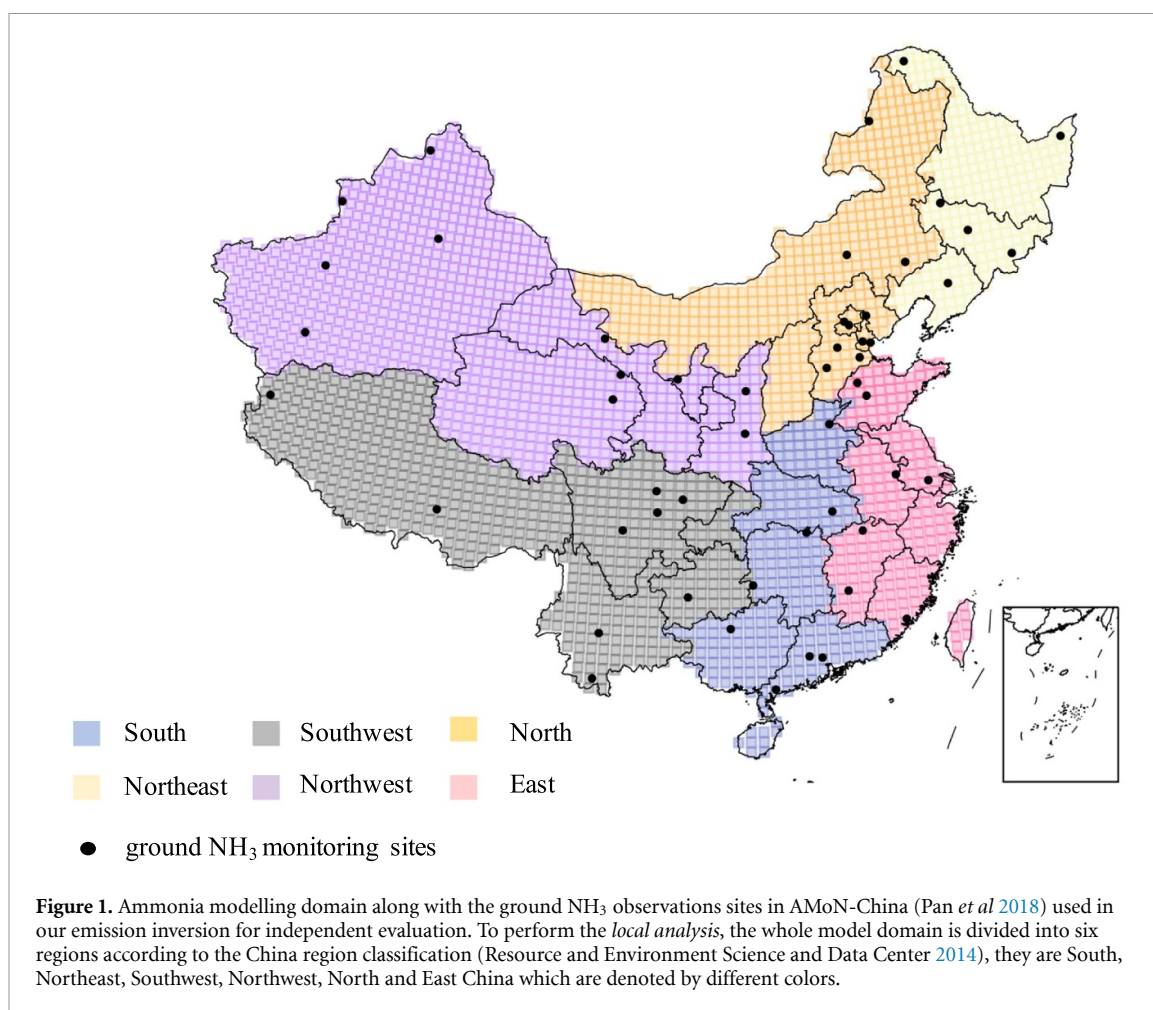
The prior  $\text{NH}_3$  emission estimates used to onward GEOS-Chem were from the Multiresolution Emission Inventory for China (MEIC, [www.meicmodel.org](http://www.meicmodel.org), last access: August 1, 2022) in the base year of 2016. MEIC is the most popular model for tracking anthropogenic emission in China. Besides the ammonia, MEIC provides other aerosol and gas pollutant emission for GEOS-Chem. In addition to the MEIC, ammonia inventory such as from Kong *et al* (2019) and Li *et al* (2021) could be served as the prior alternatively, which are actually in better harmony with our posterior as will be discussed in section 4.1. However, inputs of the continuous prior emission inventories such as from the MEIC model are required in the long-term ammonia emission inversion in our following work. Therefore, Kong *et al* (2019) and Li *et al* (2021) that focused on emission inventory in a single year are not capable of tracking the annual variations as the prior inputs, and not used in this study as well.

Ammonia is assumed to be released only from anthropogenic activities similar to other air quality modeling studies over China (Li *et al* 2021, Yan *et al* 2021), while natural sources are absent. The detailed ammonia sources included in MEIC were agriculture, industry, residential, and transportation. The majority were released from agriculture, specifically fertilizers and livestock waste (Li *et al* 2021). The MEIC emission estimates were coarsened before they were used to forward the GEOS-Chem simulation. The coarsened emission inventory was taken as the average over the  $0.5^\circ \times 0.625^\circ$  model grid cell. A snapshot of the coarsened monthly ammonia emission flux in April, July, and October of 2016 is shown in figures 2(a.1)–(a.3).

For ammonia out of China, the emission is from global anthropogenic emissions of the CEDS inventory (Hoesly *et al* 2018). Although emissions out of China also contribute partially to domestic atmospheric ammonia, especially over the boundary regions, their contribution is assumed to be certain and hence will not be optimized here.

### 2.3. IASI satellite measurements

The IASI is a Fourier transform infrared sounder onboard the Sun-synchronous orbiting satellites Meteorological Operational satellite A/B/C (Metop-A/B/C), which were launched in 2008, 2012, and 2018, respectively. Each IASI instrument enables bi-daily measurements of a series of atmospheric pollutants passing by between 09:30 and 21:30 (local time). The IASI has a relatively high spatial resolution (12 km at the nadir) and a swath width of  $2 \times 1100$  km (Clerbaux *et al* 2009). The ammonia retrieval algorithm of the IASI has been steadily



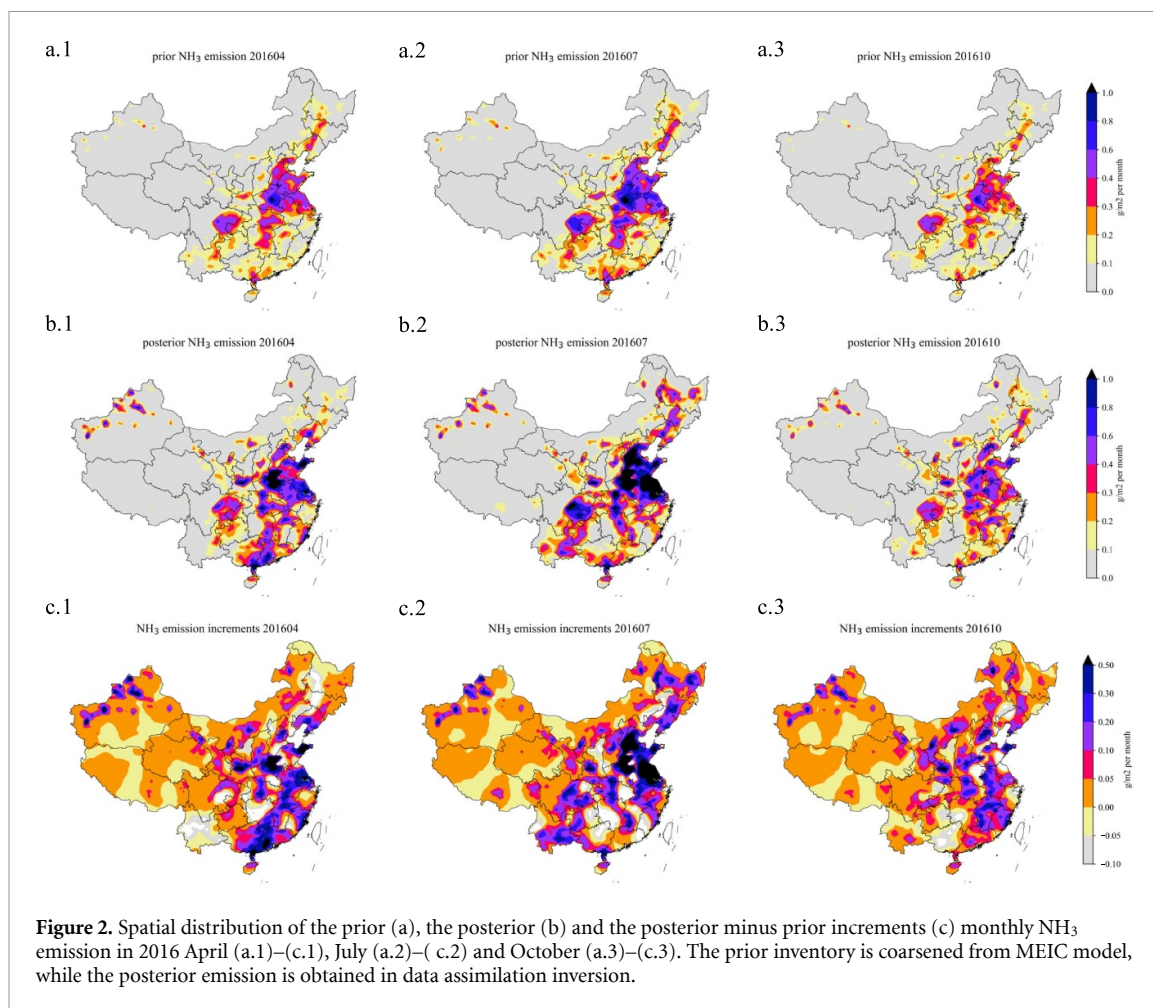
improved. The initial product used lookup tables based on simulations of a forward radiative transfer model (Van Damme et al 2014). An artificial neural network was then applied for ammonia retrieval in IASI version 1 (Whitburn et al 2016). As infrared retrievals are known to be sensitive to auxiliary input, an additional IASI product was released in updated version 2, which used the temperature data from ECMWF ERA-Interim instead of using meteorological input from IASI itself (Van Damme et al 2017). The latest release of the IASI (version 3) (ANNI-NH3-v3R-ERA5) from Metop-A/B was used for ammonia emission inversion in our study. This version builds on the heritage of versions 1 and 2, and further advances have been made in the neural network retrieval, outlined in Franco et al (2019).

Regardless of the improvement of NH<sub>3</sub> column retrieval from satellite observations, there is still substantial variability in measurement uncertainty, varying from 5% to over 1000% (Van Damme et al 2017). Considering the relatively high uncertainty in infrared retrievals and the high data missing rate over clouded scenes, IASI products are insufficient and rarely used for real-time ammonia monitoring, although their monthly averages are sufficient (Ge et al 2020). Similarly, the monthly means over the  $0.5^\circ \times 0.625^\circ$  GEOS-Chem grid cell were derived

based on the raw ANNI-NH3-v3R-ERA5 product. Meanwhile, data selection was used by excluding irrational observed values ( $<0$ ) in the monthly average calculation. Snapshots of the coarse IASI ammonia monthly average in April, July, and October 2016, are shown in figures 3(a.1)–(a.3).

The goal of this study was to estimate ammonia emissions through assimilation of coarse IASI ammonia column observations. To achieve this, it is necessary to describe the uncertainty in the measurements to quantify the observation-minus-simulation mismatch, as will be discussed in section 3.1. Instrument  $\sigma^{\text{instrument}}$  and representing errors  $\sigma^{\text{representing}}$  were considered when the uncertainty of the gridded monthly average ammonia measurements were calculated. The gridded mean of the uncertainties directly taken from the IASI product was treated as the instrument error  $\sigma^{\text{instrument}}$ , whereas the standard deviation of the observation samples for calculating the grid average was used to characterize the representing error  $\sigma^{\text{representing}}$ . The integrated uncertainty  $\sigma^{\text{integrated}}$  for using the coarsened IASI ammonia measurements to represent the atmospheric ammonia intensity was then calculated as:

$$\sigma^{\text{integrated}} = \{(\sigma^{\text{instrument}})^2 + (\sigma^{\text{representing}})^2\}^{0.5}. \quad (1)$$



Spatial distribution of the uncertainty with respect to the IASI ammonia column observations in figures 3(a.1)–(a.3) could also be found in figures 3(b.1)–(b.3).

#### 2.4. Surface ammonia measurements

The monthly surface concentration from the ammonia monitoring network in China (AMoN-China) established by Pan *et al* (2018) was used as an independent measurement for the assimilation evaluation in this study. AMoN-China has 53 monitoring sites on a national scale, which are marked in figure 1. A year-round observational campaign was launched between September 2015 and August 2016. Observation of the spatial variability of atmospheric ammonia was based on uniform protocols using a diffusive technique. Surface ammonia concentration observations in April and July 2016 were then used to evaluate improvements in ammonia simulation using emission inversion.

### 3. Emission inversion system

This study aimed to develop a top-down ammonia emission estimation system by assimilating the IASI measurements described above into the GEOS-Chem model. The system used a 4DENVAR assimilation

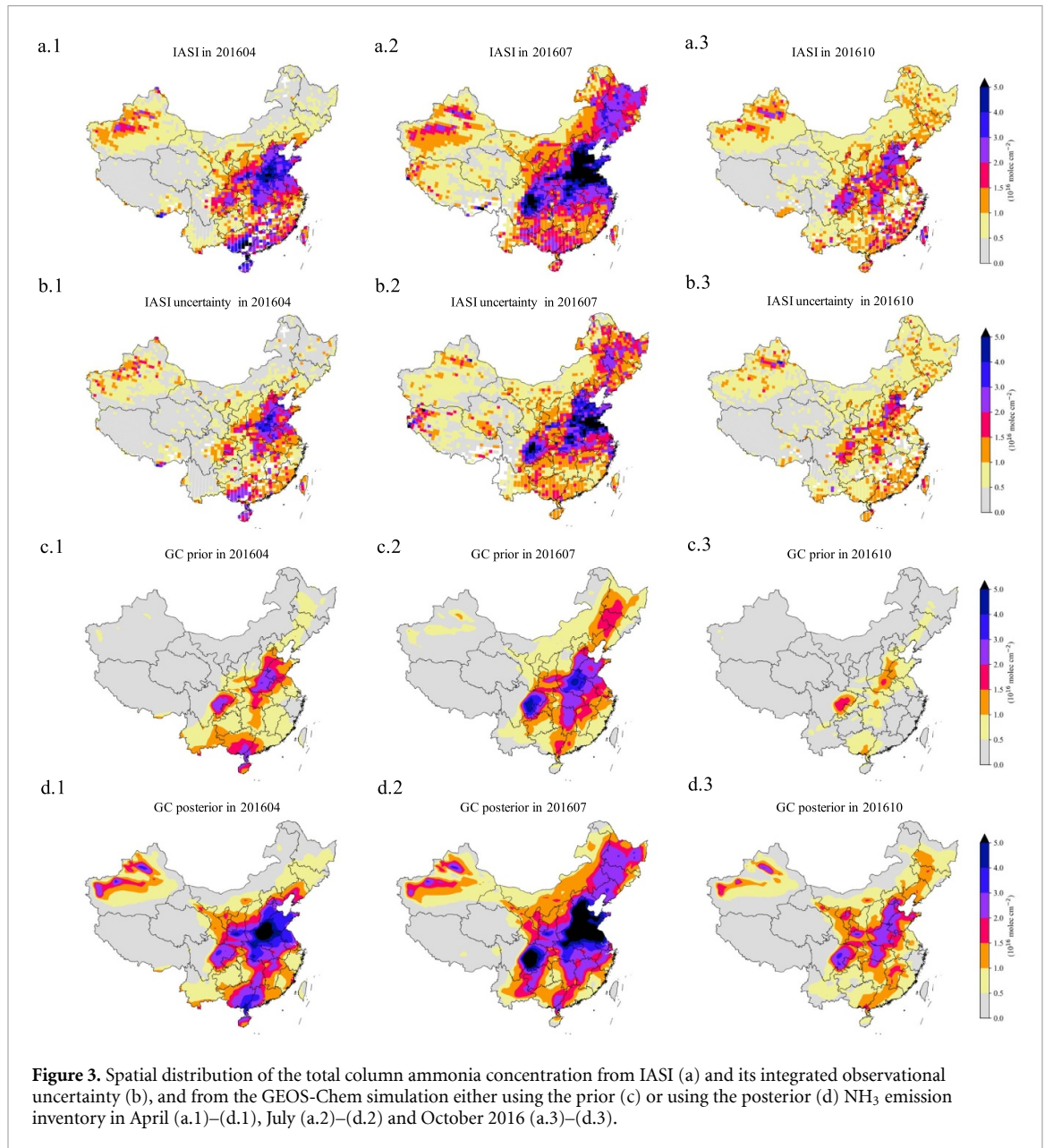
algorithm to nudge the monthly ammonia emission inventory. Local analysis was used to better represent the covariance statistics with limited ensemble members.

#### 3.1. Assimilation algorithm

The 4DENVAR assimilation algorithm was first proposed by Liu *et al* (2008) and successfully implemented in our recent dust storm emission inversion (Jin *et al* 2021). The goal of this assimilation is to find the most likely estimate of a state vector, which is the monthly ammonia emission inventory  $\mathbf{f}$  over whole model domain, given the prior guess  $\mathbf{f}_b$  which is from MEIC model as described in section 2.2 and the available monthly IASI column observations  $\mathbf{y}$  as described in section 2.3. Theoretically, assimilation is performed by minimizing the cost function  $\mathcal{J}$ :

$$\mathcal{J}(\mathbf{f}) = \frac{1}{2}(\mathbf{f} - \mathbf{f}_b)^T \mathbf{B}^{-1}(\mathbf{f} - \mathbf{f}_b) + \frac{1}{2}\{\mathbf{y} - \mathbf{H}\mathcal{M}(\mathbf{f})\}^T \times \mathbf{O}^{-1}\{\mathbf{y} - \mathbf{H}\mathcal{M}(\mathbf{f})\} \quad (2)$$

here  $\mathcal{J}$  is sum of two parts: the left term quantifies the penalty of deviation from the prior emission inventory whereas the right term calculates the discrepancy from measurement. In the background term,  $\mathbf{f}_b$  represents the prior ammonia emission inventory, which is here from MEIC as described in section 2.2.



The uncertainty in the ammonia simulation is assumed to be attributed to errors in the emission inventory, and can be compensated using a spatially varying tuning factor  $\alpha$ :

$$f(i) = f_b(i) \cdot \alpha(i) \quad (3)$$

in here  $f_b(i)$  denotes the ammonia emission rate in the given grid cell  $i$ . The  $\alpha$  values are defined to be random variables with a mean of 1.0 and a standard deviation  $\sigma_\alpha = 0.2$ . This empirical values was found to provide sufficient spaces for resolving the observation-minus-simulation errors. A background covariance  $\mathbf{B}_\alpha$  is formulated as a product of the constant standard deviation and a spatial correlation matrix  $\mathbf{C}$ :

$$\mathbf{B}_\alpha(i, j) = \sigma_\alpha \cdot \mathbf{C}(i, j) \quad (4)$$

where  $\mathbf{C}(i, j)$  represents a distance-based spatial correlation between two  $\alpha$ s in the grid cell  $i$  and  $j$ , and is defined as:

$$\mathbf{C}(i, j) = e^{-(d_{i,j}/l)^2/2} \quad (5)$$

where  $d_{i,j}$  represents the distance between two grid cells  $i$  and  $j$ .  $l$  here denotes the correlation length scale which controls the spatially variability freedom of the  $\alpha$ s. A small  $l$  means more errors in fine scale could be resolved using the assimilation, while however requires more ensemble runs to represent the model realization from emission to simulation as will be explained later. An empirical parameter  $l = 300$  km which is used in Jin *et al* (2022) to nudge the dust emission that has a rapid spatially variability is also taken in this study. To improve the effectiveness of the limited ensemble, local analysis is conducted as will be illustrated later. With the covariance matrix

$\mathbf{B}_\alpha$ , the ammonia emission background covariance  $\mathbf{B}$  is obtained via a Schur Product:

$$\mathbf{B} = \mathbf{B}_\alpha \circ \mathbf{C}. \quad (6)$$

In the observational term in equation (2),  $y$  is the observation vector that stores the coarsened IASI ammonia columns as has been described in section 2.3,  $\mathcal{M}$  is the GEOS-Chem model that driven by the emission  $f$  and  $\mathbf{H}$  is the linear observational operator that transfer the model simulation (3D ammonia concentrations) into the observational space (total columns),  $\mathbf{O}$  is here for weighting the observational mismatch. The observation uncertainty are assumed to be independent, therefore  $\mathbf{O}$  is a diagonal matrix. We have used the integrated uncertainty of the IASI columns calculated in section 2.3 with the error inflated for the low-values measurements  $\mathbf{O}_{i,i} = \max(1.0 \times 10^{16} \text{ molec cm}^{-2}, \sigma^{\text{integrated}})^2$  to characterize the IASI column observations. The minimum uncertainty here is to prevent the posterior from getting too close to the low-value observations and hence become model divergent.

The posterior ammonia inventory  $f$  is calculated by minimizing the cost function in equation (2) follows the 4D-EnVar process, and the detailed procedures are illustrated in section ‘Cost function minimization in 4D-EnVar’ in supplementary material.

### 3.2. Local analysis

The ensemble method is widely used to represent the covariance statistics of targeted problematic parameters in geo-scientific modeling. For a given space, a large ensemble would undoubtedly help to maintain the spatial or temporal variability and subsequently better represent the model dynamics, which also requires more computational power to forward these ensembles. A local analysis approach was then proposed, which facilitated a high-dimensional estimate of the global background error covariance based on a small ensemble (Ott *et al* 2004). In particular, for atmospheric ammonia that photo-dissociates readily and has a short atmospheric residence time, the uncertainty in the simulation tends to lie in a subspace of much lower dimensions than the full atmospheric space. To obtain a better representation of the ammonia emission spatial variability on a fine scale, local analysis was implemented.

The local analysis algorithm is outlined as follows:

- The full model domain was categorized into six subspaces, including South, Northeast, Southwest, Northwest, North, and East China as shown in figure 1, according to the China region classification (Resource and Environment Science and Data Center 2014). The prior emission inventory and background error covariance were independently established for each region. Local ensembles were obtained with the regional prior and covariance.

- The ensemble emission inventory was generated in full space via combining the local ensembles, and then forward the ensemble models.
- Data assimilation was performed in each of the six low-dimensional subspaces and the posterior emission was obtained in each local region.
- The posteriors in the full model domain were established by combining six local posteriors.

## 4. Results and discussion

To test the performance of the top-down ammonia emission inversion system, monthly emission estimation experiments were conducted in each season, which are April, July, and October 2016 here. The reason why we skip the winter season is IASI data product has relatively large errors in cold time as the retrieval algorithm is highly sensitive to temperature inputs (Ge *et al* 2020). A snapshot of the January 2016 IASI ammonia monthly averaged measurement in the winter season are presented in figure S1. Notably, much less data coverage is found there, especially in the Northeast and Southeast China. One of the reasons for the modeling period in 2016 is the availability of emission results from related studies and surface ammonia concentration data from AMoN-China for independent evaluation. Investigations of annual and seasonal ammonia emission variations over the past decade will be conducted in our future work.

### 4.1. NH<sub>3</sub> emission

Through assimilating the IASI ammonia columns into the GEOS-Chem model, the monthly emission inventory covering the three test months are updated, which could be found in figures 2(b.1)–(b.3), and the increments are plotted in figures 2(c.1)–(c.3) as well. Our top-down posterior emissions show a very similar pattern to the prior emissions from MEIC shown in panel (a), but the intensity increased all over China in general. As shown in figures 2(c.1)–(c.3), the largest positive increment is presented in East China, which is as high as  $0.5 \text{ g m}^{-2}$  in July. The missing ammonia source in the prior MEIC model there is likely to due to the underestimation of livestock waste and fertilizer application as indicated by (Li *et al* 2021). In addition, the absence of natural ammonia sources might partially account for the underestimation in the prior inventory. Besides, ammonia emission is steadily underrated in North China Plain (NCP) which is the most severe haze-polluted region in China. The posterior ammonia emission inventory not only brought the ammonia concentration in better harmony with the measurements, but also resulted a more accurate aerosol simulation in NCP as will be discussed later.

Based on the prior inventory shown in figure 2(a), ammonia emission in Xinjiang Province in Northwest China was almost negligible and there were very limited grid cells with emission flux reaching



**Table 1.** Regional monthly NH<sub>3</sub> emission (10<sup>5</sup> tons).

Region	201604				201607				201610			
	<i>Li21</i>	<i>Kong19</i>	Prior	Posterior	<i>Li21</i>	<i>Kong19</i>	Prior	Posterior	<i>Li21</i>	<i>Kong19</i>	Prior	Posterior
Northeast	0.92	—	0.83	0.93	1.7	—	1.0	1.8	0.6	—	0.68	0.88
North	1.9	—	1.1	1.6	2.5	—	1.3	2.5	1.3	—	0.88	1.6
East	2.2	—	1.7	3.0	3.4	—	2.3	4.3	1.8	—	1.4	2.3
Northwest	1.7	—	0.81	1.9	2.1	—	1.0	1.9	1.1	—	0.65	1.6
Southwest	1.4	—	1.5	1.4	2.0	—	1.8	2.7	1.4	—	1.2	1.4
South	2.8	—	2.3	3.5	3.3	—	2.9	3.7	2.2	—	1.8	2.1
China	11.0	11.1	8.3	12.3	15.0	17.2	10.3	16.9	8.4	—	6.61	9.9

—: data is unavailable.

0.1 g m<sup>-2</sup> monthly. Given the low uncertainty shown in figures 3(b.1)–(b.3), however, the IASI instruments were very confident that there are unignorable ammonia pollutants seen in figures 3(a.1)–(a.3). Ammonia emissions were then nudged several times higher to better fit the observations. However, the nonlinearity from the emission to the ammonia load was not fully reproduced using the ensemble models, which led to a slight overestimation, as explained later.

The emission budgets collected from Li *et al* (2021) and from Kong *et al* (2019) are used to evaluate our posterior emission inventory. The former (referred to as *Li21*) was obtained through improving fertilizer-related ammonia allocation in a bottom-up way, while the latter (referred to as *Kong19*) was obtained through assimilating the AMoN-China surface measurements. In the most severe summer season July, the total emission flux in our posterior estimate increased to 16.9 (×10<sup>5</sup> tons m<sup>-1</sup>), which is 55.3% higher than the prior estimate (see table 1). This is also much more consistent with the emission estimation 15.0 (×10<sup>5</sup> tons m<sup>-1</sup>) from (Li *et al* 2021) and 17.2 (×10<sup>5</sup> tons m<sup>-1</sup>) from Kong *et al* (2019). The emission increments were heterogeneous in different regions, and significant increases were found in the Northeast, North, East, Northwest and Southwest, with a minimum increase of 50%. Northwest China had the largest increase of approximately 95%. Our regional ammonia estimations are consistent with those reported by Li *et al* (2021) especially in Northeast, North, and Northwest China. The high consistency between our top-down source estimates and bottom-up inventories from Li *et al* (2021) suggested more efforts should be made to the fertilizer-related emissions while building the ammonia inventory. In the spring and autumn seasons, our assimilation also resulted in a posterior that agrees better with the values reported by *Li201* and *Kong19*.

The posterior calculated in the assimilation has the least deviation from both the prior ammonia emission inventory and the IASI column concentrations, which are quantified by the background and observational penalty shown in equation (2). For the tested three months in 2016, different priors such as the benchmarks *Li201* and *Kong19* could

be used alternatively. These priors with less bias and an appropriate background covariance matrix **B** are likely to result in a more promising posterior as illustrated in our dust assimilation work (Jin *et al* 2020). The difference using various priors are supposed to be slight when the measurements with a huge size are dominant in the cost function as indicated in our aerosol optical property assimilation (Jin *et al* 2023).

#### 4.2. NH<sub>3</sub> total column concentration

The GEOS-Chem simulated total columns, either using the prior or posterior ammonia estimates over the three periods, as shown in figures 3(c) and (d). The prior result in panel (a) shows a relatively similar spatial distribution to the observed columns, as shown in figure 3(a). Most of the hotspots of ammonia pollution in East, Southwest, and South China were well reproduced by the priors. According to the scatter plots of the observation versus the prior simulation shown in figure 4, the prior resulted in high *Pearson* correlations (*r*) with 0.802 in April, 0.806 in July and 0.661 in October. However, the prior generally underrated the actual ammonia loads, which was significantly improved in the posterior simulation in figure 3(d) by assimilating the IASI columns. The observation-minus-simulation discrepancies (root mean square error, RMSE) were efficiently reduced to 0.504, 0.648, and 0.472 (×10<sup>5</sup> tons/month), which were 33.7, 44.7, and 38.1% lower than in the prior simulations. The correlation coefficients *r* further increased to 0.879, 0.902, and 0.745, synchronously.

The posterior ammonia emission estimates also improve the PM<sub>2.5</sub> simulation indirectly. The best example could be seen supplementary figure S2. Panel (a.1) there illustrated our GEOS-Chem generally underrated the PM<sub>2.5</sub> pollution in the summer season. The increase of atmospheric ammonia in our posterior model simulation facilitated the formation of the secondary fine aerosols, and resulted in a heterogeneous increment of the PM<sub>2.5</sub> simulation as shown in panel (b.1). This partially reduced the PM<sub>2.5</sub> simulation errors in GEOS-Chem over the whole China domain with the RMSE declined from 13.9 to 13.4 μg m<sup>-3</sup> as shown in panels (a.2) to (b.2). Over the most severe polluted region NCP,

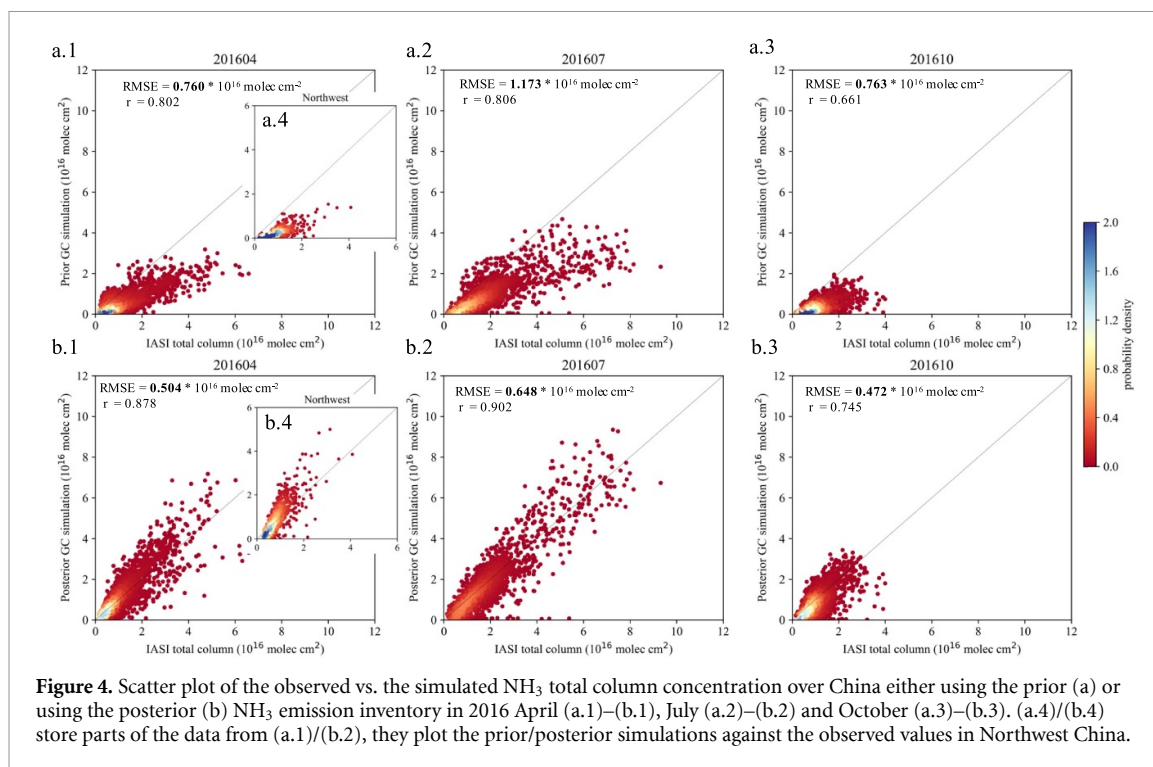


**Figure 4.** Scatter plot of the observed vs. the simulated  $\text{NH}_3$  total column concentration over China either using the prior (a) or using the posterior (b)  $\text{NH}_3$  emission inventory in 2016 April (a.1)–(b.1), July (a.2)–(b.2) and October (a.3)–(b.3). (a.4)/(b.4) store parts of the data from (a.1)/(b.2), they plot the prior/posterior simulations against the observed values in Northwest China.

the posterior ammonia emission further improves the aerosol simulation, where the RMSE is efficiently reduced from  $12.8$  to  $10.9 \mu\text{g m}^{-3}$ . Student's  $t$ -tests (Ni *et al* 2017) were further carried out to examine these observation-minus-simulation errors, which confirmed the obvious improvements ( $p < 0.001$ ) in the posterior  $\text{PM}_{2.5}$  simulation both over the whole China domain and NCP.

The GEOS-Chem simulation driven by the posterior is brought to be in better harmony with the IASI ammonia retrievals using the posterior, however, the errors still remains partially. One reason is that the ensemble emission spreads in equation (1) in the supplement (e.g.  $N = 16$  in this study) might be insufficient to represent the very local emission covariance statistics. In addition, the essence of 4DEnVar assimilation algorithm is to emulate the GEOS-Chem ammonia simulating model using an ensemble-based linear approximation, which might cause a loss of the original model non-linearity to some degree, especially when the background error covariance is severely underestimated or overestimated. In this study, the standard deviation ( $\sigma_\alpha$ ) of the emission tuning factor is set as 0.2 constantly, and it is capable of resolving the emission errors over most regions. However, there is a very strong negative bias in the prior simulation in Xinjiang Province as can be seen in figure 4(a.4) that plots the scatter distribution of the observations vs. the simulation over Northwest China. The actual values (like observations) are several times higher than the simulated results, and fall outside the range defined with  $\sigma_\alpha = 0.2$ . It will therefore lead to an inaccurate assimilation result which is here the overestimation seen in figure 4(b.4). These

two issues might be partially addressed by using larger ensemble member and adding additional iteration loops, e.g. iteratively resampling ensemble of emission inventory and forming new linear approximations at the outer-loops as suggested by Nakano (2021). These however will severely increase the computational cost and thus challenge the inversion of long-term ammonia emission estimates over China.

### 4.3. $\text{NH}_3$ surface concentration

The ammonia emission inversion was further evaluated using the independent surface ammonia concentration data retrieved from AMoN-China. As shown in figure 5, the GEOS-Chem ammonia surface concentration simulations driven by the posterior emission inventory (panels (b.1) and (b.2)) better agree with the spatial distributions of the measurements compared to the prior result (panels (a.1) and (a.2)). The negative bias in the prior surface ammonia concentration simulation for April and July shown in figure 5(a.3) was improved, with the RMSE declined from  $10.06 \mu\text{g m}^{-3}$  to  $8.10 \mu\text{g m}^{-3}$ . Student's  $t$ -test was also conducted, which shows that there is more than a 99.9% probability ( $p < 0.001$ ) the observation-minus-simulation discrepancy is significantly reduced through using the posterior inventory.

The improvement in the surface concentration simulation was less than that obtained in the ammonia column concentration modeling, and a negative bias still exists, as shown in figure 5(b.3). A potential reason for this is that our simulation was the average ammonia load over the coarse grid cell ( $0.5^\circ$  by  $0.625^\circ$ ). However, ground-based

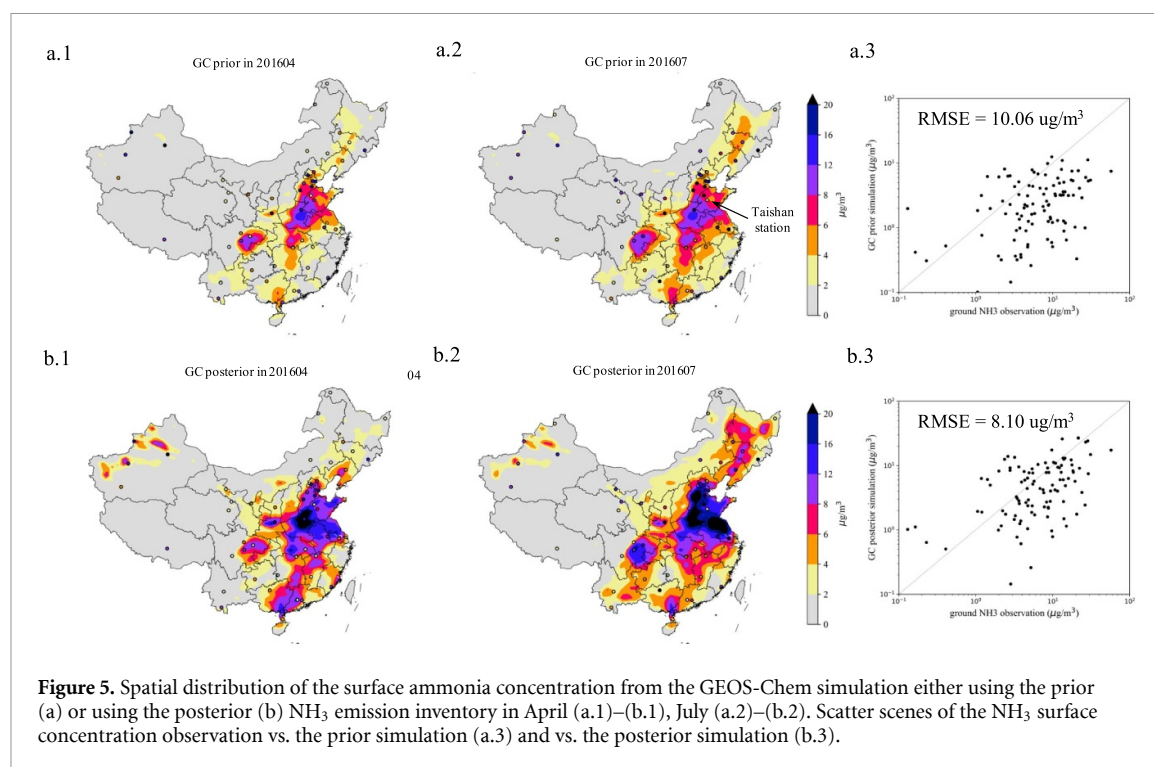


**Figure 5.** Spatial distribution of the surface ammonia concentration from the GEOS-Chem simulation either using the prior (a) or using the posterior (b)  $\text{NH}_3$  emission inventory in April (a.1)–(b.1), July (a.2)–(b.2). Scatter scenes of the  $\text{NH}_3$  surface concentration observation vs. the prior simulation (a.3) and vs. the posterior simulation (b.3).

monitoring sites measured the surrounding status might differ significantly from the grid average. Representation errors exist avoidably while the simulated value is compared to the surface observation. For instance, Taishan station ( $117.1^\circ \text{ E}$ ,  $36.3^\circ \text{ E}$ ), which is in a severely polluted area, as shown in the IASI measurements in figure 3(a.2), reported a low-level ammonia concentration ( $2.6 \mu\text{g m}^{-3}$ ) in July as marked in figure 5(a.2). The large mismatch is because the station was located on a mountain at an elevation of 1506 m; hence, the measurements collected had a strong bias for representing the average in the coarse grid. Therefore, the remaining errors in the comparison were unavoidable. To fully represent ammonia features observed in these ground sites, a model simulation with an extremely fine resolution is required which however will make the ensemble-based emission inversion unaffordable.

## 5. Summary and conclusion

The past decades have experienced an increase in atmospheric ammonia emissions in China, which has caused severe environmental and health concerns. However, current bottom-up emission inventories are highly uncertain and cannot accurately reflect the spatiotemporal distribution of the ammonia emission. Top-down emission inversion by assimilating measurements from recently developed satellite instruments, such as IASI and CrIS, has become a powerful method for exploring ammonia emissions, but such studies in China are limited.

This study developed a 4D-EnVar-based emission inversion system to optimize ammonia emissions

in China. The top-down estimation system was constructed by feeding ammonia retrievals from the IASI onboard the polar-orbiting satellites Metop-A/B into the chemical transport model GEOS-Chem. Ammonia emission inversion tests were performed in April, July, and October 2016. The inversion results indicate that: The prior inventory from the MEIC model generally captured the ammonia distribution; however, it heterogeneously underrated their intensity. Significant increments ( $>50\%$ ) were observed by assimilation in North, East, and Northwest China. These results were also consistent with the values obtained in an improved agriculture-based bottom-up inventory and a top-down estimate that assimilated surface ammonia concentration.

Driven by the posterior emission inventory, the GEOS-Chem-simulated total ammonia columns concurred with the IASI measurements. Favorable posterior simulations were obtained with 33.7%, 44.7%, and 38.1% lower RMSEs and relatively high correction coefficients (0.878, 0.902, and 0.745) in April, July, and October, respectively. Superior results were obtained by comparing the independent surface ammonia concentrations from China-AMoN.

This promising performance gives us confidence to explore the characteristics of ammonia emissions in China, for example, annual, seasonal, and detailed spatial variability in the past decade, by assimilating the IASI measurements in the near future. However, a space for improving the emission inversion system also exists. For instance, logarithmic amplifiers should be considered while building tuning factors for emissions when a very strong negative bias is present. In addition, the other advanced ammonia

satellite product CrIS deserves attention, which will be considered for assimilation together with IASI data in our future work.

### Code and data availability

The ammonia emission inversion system is in the Python environment and is archived on Zenodo (<https://doi.org/10.5281/zenodo.7015397>; Jianbing Jin, 2022). The IASI ANNI-NH<sub>3</sub>-v3R-ERA5 data suites are available at <https://iasi.aeris-data.fr/>. The observed NH<sub>3</sub> concentrations data (AMoN-China) is published by Pan *et al* (2018) from Institute of Atmospheric Physics, Chinese Academy of Sciences.

### Funding statement

This work is supported by the National Natural Science Foundation of China (Grant Nos. 42105109 and 42021004) and Natural Science Foundation of Jiangsu Province (Grant Nos. BK20210664 and BK20220031).


### Conflict of interest

The authors declare that they have no conflict of interest.

### ORCID iDs

Jianbing Jin  <https://orcid.org/0000-0002-2868-9343>

Ke Li  <https://orcid.org/0000-0002-9181-3562>

Mijie Pang  <https://orcid.org/0000-0001-9773-0488>

Hai Xiang Lin  <https://orcid.org/0000-0002-1653-4854>

### References

- Bier R *et al* 2008 First satellite observations of lower tropospheric ammonia and methanol *Geophys. Res. Lett.* **35** L09801
- Cao H *et al* 2020 Inverse modeling of NH<sub>3</sub> sources using CrIS remote sensing measurements *Environ. Res. Lett.* **15** 104082
- Cao H *et al* 2022 4D-Var inversion of European NH<sub>3</sub> emissions using CrIS NH<sub>3</sub> measurements and GEOS-Chem adjoint with bi-directional and uni-directional flux schemes *J. Geophys. Res. Atmos.* **127** e2021JD035687
- Chen Y *et al* 2021 High-resolution hybrid inversion of IASI ammonia columns to constrain US ammonia emissions using the CMAQ adjoint model *Atmos. Chem. Phys.* **21** 2067–82
- Clarisse L, Clerbaux C, Dentener F, Hurtmans D and Coheur P-F 2009 Global ammonia distribution derived from infrared satellite observations *Nat. Geosci.* **2** 479–83
- Clerbaux C *et al* 2009 Monitoring of atmospheric composition using the thermal infrared IASI/MetOp sounder *Atmos. Chem. Phys.* **9** 6041–54
- Crippa M *et al* 2018 Gridded emissions of air pollutants for the period 1970–2012 within EDGAR v4. 3.2 *Earth Syst. Sci. Data* **10** 1987–2013
- Franco B, Clarisse L, Stavrou T, Müller J-F, Pozzer A, Hadji-Lazarou J, Hurtmans D, Clerbaux C and Coheur P-F 2019 Acetone atmospheric distribution retrieved from space *Geophys. Res. Lett.* **46** 2884–93
- Ge X, Schaap M, Kranenburg R, Segers A, Reinds G J, Kros H and de Vries W 2020 Modeling atmospheric ammonia using agricultural emissions with improved spatial variability and temporal dynamics *Atmos. Chem. Phys.* **20** 16055–87
- Gelaro R *et al* 2017 The modern-era retrospective analysis for research and applications, version 2 (MERRA-2) *J. Clim.* **30** 5419–54
- Guo X *et al* 2021 Validation of IASI satellite ammonia observations at the pixel scale using in situ vertical profiles *J. Geophys. Res. Atmos.* **126** e2020JD033475
- Hernández D L, Vallano D M, Zavaleta E S, Tzankova Z, Pasari J R, Weiss S, Selmants P C and Morozumi C 2016 Nitrogen pollution is linked to US listed species declines *BioScience* **66** 213–22
- Hoesly R M *et al* 2018 Historical (1750–2014) anthropogenic emissions of reactive gases and aerosols from the Community Emissions Data System (CEDS) *Geosci. Model Dev.* **11** 369–408
- Huang R-J *et al* 2014 High secondary aerosol contribution to particulate pollution during haze events in China *Nature* **514** 218–22
- Huang X, Song Y, Li M, Li J, Huo Q, Cai X, Zhu T, Hu M and Zhang H 2012 A high-resolution ammonia emission inventory in China *Glob. Biogeochem. Cycles* **26** GB1030
- Jin J, Henzing B and Segers A 2023 How aerosol size matters in aerosol optical depth (AOD) assimilation and the optimization using the Ångström exponent *Atmos. Chem. Phys.* **23** 1641–60
- Jin J, Pang M, Segers A, Han W, Fang L, Li B, Feng H, Lin H X and Liao H 2022 Inverse modeling of the 2021 spring super dust storms in East Asia *Atmos. Chem. Phys.* **22** 6393–410
- Jin J, Segers A, Liao H, Heemink A, Kranenburg R and Lin H X 2020 Source backtracking for dust storm emission inversion using an adjoint method: case study of Northeast China *Atmos. Chem. Phys.* **20** 15207–25
- Jin J, Segers A, Lin H X, Henzing B, Wang X, Heemink A and Liao H 2021 Position correction in dust storm forecasting using LOTOS-EUROS v2.1: grid-distorted data assimilation v1.0 *Geosci. Model Dev.* **14** 5607–22
- Kalnay E 2002 *Atmospheric Modeling, Data Assimilation and Predictability* (Cambridge: Cambridge University Press)
- Kang Y *et al* 2016 High-resolution ammonia emissions inventories in China from 1980 to 2012 *Atmos. Chem. Phys.* **16** 2043–58
- Kong L *et al* 2019 Improved inversion of monthly ammonia emissions in China based on the Chinese ammonia monitoring network and ensemble Kalman filter *Environ. Sci. Technol.* **53** 12529–38
- Krupa S 2003 Effects of atmospheric ammonia (NH<sub>3</sub>) on terrestrial vegetation: a review *Environ. Pollut.* **124** 179–221
- Kurokawa J, Ohara T, Morikawa T, Hanayama S, Janssens-Maenhout G, Fukui T, Kawashima K and Akimoto H 2013 Emissions of air pollutants and greenhouse gases over Asian regions during 2000–2008: Regional Emission inventory in ASia (REAS) version 2 *Atmos. Chem. Phys.* **13** 11019–58
- Li B, Chen L, Shen W, Jin J, Wang T, Wang P, Yang Y and Liao H 2021 Improved gridded ammonia emission inventory in China *Atmos. Chem. Phys.* **21** 15883–900
- Liu C, Xiao Q and Wang B 2008 An ensemble-based four-dimensional variational data assimilation scheme. Part I: technical formulation and preliminary test *Mon. Weather Rev.* **136** 3363–73
- Liu H, Jacob D J, Bey I and Yantosca R M 2001 Constraints from 210Pb and 7Be on wet deposition and transport in a global three-dimensional chemical tracer model driven by assimilated meteorological fields *J. Geophys. Res. Atmos.* **106** 12109–28
- Myhre G *et al* 2013 Radiative forcing of the direct aerosol effect from AeroCom Phase II simulations *Atmos. Chem. Phys.* **13** 1853–77
- Nakano S 2021 Behavior of the iterative ensemble-based variational method in nonlinear problems *Nonlinear Process. Geophys.* **28** 93–109

- Ni H *et al* 2017 PM<sub>2.5</sub> emissions and source profiles from open burning of crop residues *Atmos. Environ.* **169** 229–37
- Ott E, Hunt B R, Szunyogh I, Zimin A V, Kostelich E J, Corazza M, Kalnay E, Patil D and Yorke J A 2004 A local ensemble Kalman filter for atmospheric data assimilation *Tellus A* **56** 415–28
- Pan Y *et al* 2018 Identifying ammonia hotspots in China using a national observation network *Environ. Sci. Technol.* **52** 3926–34
- Park R J, Jacob D J, Field B D, Yantosca R M and Chin M 2004 Natural and transboundary pollution influences on sulfate-nitrate-ammonium aerosols in the United States: implications for policy *J. Geophys. Res. Atmos.* **109** D15204
- Paulot F, Jacob D J, Pinder R, Bash J, Travis K and Henze D 2014 Ammonia emissions in the United States, European Union and China derived by high-resolution inversion of ammonium wet deposition data: interpretation with a new agricultural emissions inventory (MASAGE\_NH<sub>3</sub>) *J. Geophys. Res. Atmos.* **119** 4343–64
- Resource and Environment Science and Data Center 2014 *Regional Classification in China* (available at: [www.resdc.cn/data.aspx?DATAID=276](http://www.resdc.cn/data.aspx?DATAID=276))
- Shephard M and Cady-Pereira K 2015 Cross-track Infrared Sounder (CrIS) satellite observations of tropospheric ammonia *Atmos. Meas. Tech.* **8** 1323–36
- Sitwell M, Shephard M W, Rochon Y, Cady-Pereira K and Dammers E 2022 An ensemble-variational inversion system for the estimation of ammonia emissions using CrIS satellite ammonia retrievals *Atmos. Chem. Phys.* **22** 6595–624
- Van Damme M, Clarisse L, Heald C L, Hurtmans D, Ngadi Y, Clerbaux C, Dolman A J, Erismann J W and Coheur P F 2014 Global distributions, time series and error characterization of atmospheric ammonia (NH<sub>3</sub>) from IASI satellite observations *Atmos. Chem. Phys.* **14** 2905–22
- Van Damme M, Whitburn S, Clarisse L, Clerbaux C, Hurtmans D and Coheur P-F 2017 Version 2 of the IASI NH<sub>3</sub> neural network retrieval algorithm: near-real-time and reanalysed datasets *Atmos. Meas. Tech.* **10** 4905–14
- van der Graaf S, Dammers E, Segers A, Kranenburg R, Schaap M, Shephard M W and Erismann J W 2022 Data assimilation of CrIS NH<sub>3</sub> satellite observations for improving spatiotemporal NH<sub>3</sub> distributions in LOTOS-EUROS *Atmos. Chem. Phys.* **22** 951–72
- Walker J, Philip S, Martin R and Seinfeld J 2012 Simulation of nitrate, sulfate and ammonium aerosols over the United States *Atmos. Chem. Phys.* **12** 11213–27
- Whitburn S, Van Damme M, Clarisse L, Bauduin S, Heald C, Hadji-Lazarou J, Hurtmans D, Zondlo M A, Clerbaux C and Coheur P-F 2016 A flexible and robust neural network IASI-NH<sub>3</sub> retrieval algorithm *J. Geophys. Res. Atmos.* **121** 6581–99
- Xu P, Liao Y, Lin Y, Zhao C, Yan C, Cao M, Wang G and Luan S 2016 High-resolution inventory of ammonia emissions from agricultural fertilizer in China from 1978 to 2008 *Atmos. Chem. Phys.* **16** 1207–18
- Xu R, Tian H, Pan S, Prior S A, Feng Y, Batchelor W D, Chen J and Yang J 2019 Global ammonia emissions from synthetic nitrogen fertilizer applications in agricultural systems: empirical and process-based estimates and uncertainty *Glob. Change Biol.* **25** 314–26
- Yan Y *et al* 2021 Effectiveness of emission control in reducing PM<sub>2.5</sub> pollution in central China during winter haze episodes under various potential synoptic controls *Atmos. Chem. Phys.* **21** 3143–62
- Zhang L *et al* 2018 Agricultural ammonia emissions in China: reconciling bottom-up and top-down estimates *Atmos. Chem. Phys.* **18** 339–55
- Zhang L, Gong S, Padro J and Barrie I 2001 A size-segregated particle dry deposition scheme for an atmospheric aerosol module *Atmos. Environ.* **35** 549–60
- Zhou F, Ciais P, Hayashi K, Galloway J, Kim D-G, Yang C, Li S, Liu B, Shang Z and Gao S 2016 Re-estimating NH<sub>3</sub> emissions from Chinese cropland by a new nonlinear model *Environ. Sci. Technol.* **50** 564–72